environmental microbiology

Environmental Microbiology (2012) **14**(4), 982–992 doi:10.1111/j.1462-2920.2011.02676.x

Light utilization efficiency in photosynthetic microbial mats

Mohammad A. A. Al-Najjar,[1]* Dirk de Beer,[1] Michael Kühl[2,3] and Lubos Polerecky[1]

[1]*Max-Planck Institute for Marine Microbiology, Celsiusstr.1, 28359 Bremen, Germany.*

[2]*Marine Biological Section, Department of Biology, University of Copenhagen, Copenhagen, Denmark.*

[3]*Plant Functional Biology and Climate Change Cluster, Department of Environmental Sciences, University of Technology Sydney, Sydney, New South Wales, Australia.*

Summary

Based on combined microsensor measurements of irradiance, temperature and O_2, we compared light energy budgets in photosynthetic microbial mats, with a special focus on the efficiency of light energy conservation by photosynthesis. The euphotic zones in the three studied mats differed in their phototrophic community structure, pigment concentrations and thickness. In all mats, < 1% of the absorbed light energy was conserved via photosynthesis at high incident irradiance, while the rest was dissipated as heat. Under light-limiting conditions, the photosynthetic efficiency reached a maximum, which varied among the studied mats between 4.5% and 16.2% and was significantly lower than the theoretical maximum of 27.7%. The maximum efficiency correlated linearly with the light attenuation coefficient and photopigment concentration in the euphotic zone. Higher photosynthetic efficiency was found in mats with a thinner and more densely populated euphotic zone. Microbial mats exhibit a lower photosynthetic efficiency compared with ecosystems with a more open canopy-like organization of photosynthetic elements, where light propagation is not hindered to the same extent by photosynthetically inactive components; such components contributed about 40–80% to light absorption in the investigated microbial mats, which is in a similar range as in oceanic planktonic systems.

Received 9 August, 2011; revised 8 November, 2011; accepted 20 November, 2011. *For correspondence. E-mail malnajja@mpi-bremen.de; Tel. (+49) 421 2028836; Fax (+49) 421 2028690.

Introduction

Photosynthetic mats are compacted and densely populated microbial ecosystems. Light is the primary energy source, which leads to the accumulation of organic matter in the biomass of photoautotrophic bacteria and microalgae. Excretion of photosynthates and degradation of phototrophs supports a high diversity of heterotrophic bacteria that remineralize organic matter using a variety of electron acceptors such as O_2 or sulfate, and chemolithotrophs that gain energy from reoxidation of reduced mineralization products such as sulfide (Teske and Stahl, 2001; Des Marais, 2003; Ward *et al.*, 2006). This microbially mediated energy conversion and element cycling is very intensive and occurs within a layer that is typically a few millimetres to centimetres thick (van Gemerden 1993). The close coupling of autotrophic and heterotrophic processes results in a low net growth rate ranging from < 1 to a few mm per year in most microbial mats. Most studies on photosynthetic microbial mats have focused on detailed investigation of microbial diversity, the interactions between different microbes and biogeochemical processes, and the influence of environmental conditions and mass transfer on the ecosystem structure and function (e.g. Ferris *et al.*, 1997; Epping and Kühl, 2000; Des Marais, 2003; Jonkers *et al.*, 2003; 2005; Ward *et al.*, 2006; Dillon *et al.*, 2009; Foster *et al.*, 2009). These studies show that although the structure and function are generally highly variable among photosynthetic mats from different habitats, there exists a typical pattern that is common for all of them – a pronounced vertical stratification of the microbial community and of microenvironmental conditions in the form of steep gradients of physical and chemical parameters. This stratification is a result of steep attenuation of light with depth, high volume-specific rates of metabolic activity of the different functional groups in the mat ecosystem, and the diffusion-limited transport of substrates and products of metabolic processes (Jørgensen *et al.*, 1987; Kühl *et al.*, 1996; Kühl and Fenchel, 2000; Visscher and Stolz, 2005). Besides spatial variability, large temporal fluctuations in microenvironmental conditions due to variable light availability associated with day-night cycles are also typical for photosynthetic mats, at least in and around the euphotic zone where the primary productivity occurs (Steunou *et al.*, 2008; Jensen *et al.*, 2011). Photosynthetic microbial mats

are amongst the most investigated microbial ecosystems, yet the overall energy efficiency of such purely microbial ecosystems is largely unexplored (but see Al-Najjar *et al.*, 2010).

In this study, we focus on the efficiency with which light as the primary energy source is utilized and converted to chemical energy in three photosynthetic mats originating from locations with different environmental characteristics. We followed the fate of light energy in the mats using a recently developed microsensor-based approach (Al-Najjar *et al.*, 2010). Specifically, we used microsensors for irradiance, temperature and O_2 to measure, respectively, the rates of light absorption, heat production and photosynthetic energy conservation in the system. Subsequently, we divided the respective energy fluxes with the flux of absorbed light energy to calculate the efficiencies of light energy conservation and heat dissipation as a function of the absorbed light flux. These functional measurements were supplemented with pigment analysis and microscopy to characterize the influence of structural parameters on the light energy budget in the different mats.

Results

The data presented here were obtained from photosynthetic mats originating from Abu-Dhabi (AD), the Arctic (ARC) and Australia (AUS). In the AD mat, the pigmented surface layer contained substantial amounts of sediment particles and appeared orange-red at the top and dark-green below. The ARC sample consisted of a brown-green layer covering dark-brown muddy sediment. The AUS mat contained a highly compacted dark-green layer on top of dark-brown and black sediment (Fig. S1).

Photopigments

Hyperspectral imaging of vertical mat sections revealed large differences between the vertical distributions of photopigments (Fig. 1, upper panels). All mats contained Chlorophyll *a* (Chl *a*), a light harvesting pigment characteristic of oxygenic phototrophs (*in vivo* absorption maximum ~675 nm), which was localized in the top 1–1.8 mm of the mats. Phycocyanin (PC), an accessory pigment characteristic of cyanobacteria (*in vivo* absorption maximum ~ 625 nm), was detected in the AD and AUS mats. The PC : Chl *a* ratio increased locally at depths between 1–1.2 mm in the AD mat (Fig. 1A), while the highest PC : Chl *a* ratio was found in the top 0.2–0.3 mm of the AUS mat (Fig. 1C). Besides Chl *a* and PC, significant amounts of bacteriochlorophyll *a*, which is a characteristic pigment of anoxygenic phototrophs, were detected in the deeper layers of the AD mat. Phycocyanin could not be reliably detected in the ARC mat by the hyperspectral imaging method, because it was masked by the high amounts of chlorophyll *c* (Chl *c*; *in vivo* absorption maximum ~ 630 nm), a characteristic pigment of diatoms. Nevertheless, additional microscopy observations (Fig. S2) confirmed that both cyanobacteria and diatoms were abundant in the ARC mat.

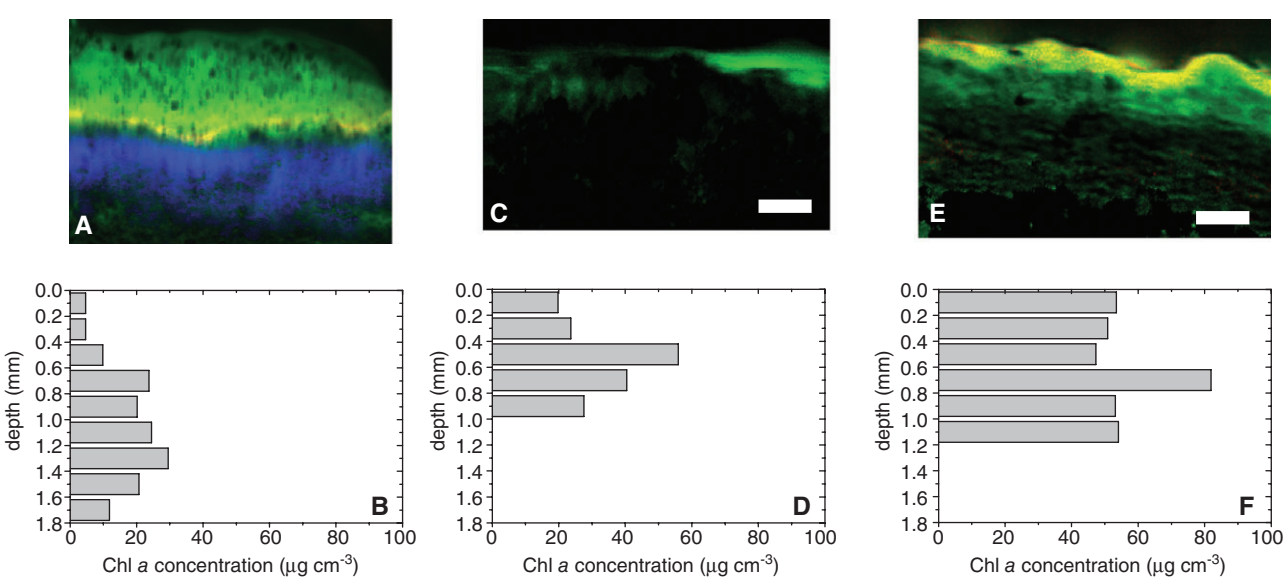

Fig. 1. Distribution of selected photopigments in the studied photosynthetic microbial mats. Composite RGB images in the upper panels show distributions of chlorophyll *a* (Chl *a*; green channel), phycocyanin (PC; red channel) and bacteriochlorophyll *a* (BChl *a*; blue channel), as derived from hyperspectral imaging based on their characteristic spectral signatures (see Fig. S1 for details). Regions characterized with high PC : Chl *a* ratio are depicted in yellow. Scale bar is 1 mm. Lower panels show vertical profiles of Chl *a* concentrations measured by high performance liquid chromatography. A and B, C and D, and E and F correspond to the AD, ARC and AUS mat respectively.

Quantitative pigment analysis by HPLC revealed that Chl *a* concentrations varied substantially among the studied mats (Fig. 1, lower panels), with the lowest and highest values found in the AD and AUS mat, respectively (Table 1). The areal Chl *a* content in the euphotic zone (see section *Photosynthesis* below) was considerably lower than the total areal Chl *a* content in the mat, which was true for all mats but especially pronounced for the AD and AUS mats. With respect to accessory photopigments, we found PC in all mats, whereas fucoxanthin (FUC), which is a characteristic pigment of diatoms, was only detected in the ARC mat. The ratio between the total content of accessory pigments and Chl *a* in the top 2 mm of the mats varied between 0.14 and 0.95 (Table 1).

Light distribution

The scalar quantum irradiance integrated over the spectral range of photosynthetically active radiation for oxygenic photosynthesis (PAR; 400–700 nm) decreased quasi exponentially with depth in the mats (Fig. 2, left panels). Light attenuation was strongest in the AUS mat and weakest in the AD mat (Table 1). Correspondingly, light penetration depths, defined as depths where scalar irradiance decreased to 1% of the value at the mat surface, ranged from 0.4 to 1 mm, and roughly coincided with the maximum thickness of the euphotic zone (Table 1).

Table 1. Functional and structural characteristics of the studied mats.

	AD	ARC	AUS
R_{PAR} (%)	17.5	5.8	1.7
$A_{PAR,mat}$ (%)	82.5	94.2	98.3
$A_{PAR,cells}$ (%)	16.4	25.8	58.3
$A_{non\text{-}PS} = 1 - A_{PAR,cells}/A_{PAR,mat}$ (%)	80.1	72.6	40.7
α (mm^{-1})	4.6	6.6	13.4
z_p (mm)	1.1	0.8	0.4
Chl *a* ($\mu g\ cm^{-3}$)	14.5	35	52
AP ($\mu g\ cm^{-3}$)	2.0	8.1	49.4
$P_{a,max}$ ($\mu mol\ O_2\ m^{-2}\ s^{-1}$)	3.9	2.9	3.0
$P_{vol,max}$ ($mmol\ O_2\ m^{-3}\ s^{-1}$)	3.3	4.1	7.6
$\varepsilon_{PS,max}$ (%)	4.5	7	16.2

R_{PAR}, mat reflectance, integrated over photosynthetically active radiation; A_{PAR}, mat absorbance, calculated as $1 - R_{PAR}$; $A_{PAR,cells}$, estimated absorbance of photosynthetically active cells in the mat; $A_{non\text{-}PS}$, estimated absorbance of photosynthetically inactive components in the mat; α, light attenuation coefficient; z_p, light penetration depth; Chl *a*, average Chlorophyll *a* concentration in the euphotic zone; AP, concentrations of accessory pigments (phycocyanin and fucoxanthin) in top 2 mm of the mat; $P_{a,max}$, areal rate of gross photosynthesis at saturating irradiance; $P_{vol,max}$, average volumetric rate of gross photosynthesis in the euphotic zone at saturating irradiance; $\varepsilon_{PS,max}$, maximum efficiency of light energy conservation by photosynthesis.

Photosynthesis

The euphotic zone, defined as the layer where gross photosynthesis was detectable with the microsensor-based light-dark shift method (Revsbech and Jørgensen, 1983), was confined to the mat surface and its thickness varied among the mats (Fig. 2, right panels). With increasing irradiance, the thickness of the photic zone increased substantially in the AD mat (from 0.4 to 1.1 mm), only slightly for the ARC mat (from 0.6 to 0.8 mm), and showed no change in the AUS mat (0.3 mm). The photosynthetic activity varied significantly with depth, reaching maxima at depths of 0.4, 0.2 and 0.1 mm for the AD, ARC and AUS mats respectively. Under saturating irradiance, the volumetric rates of gross photosynthesis were on average highest in the AUS mat (6–13 $mmol\ O_2\ m^{-3}\ s^{-1}$) and lowest in the AD mat (2–6 $mmol\ O_2\ m^{-3}\ s^{-1}$), whereas maximal areal rates of gross photosynthesis were similar for all mats (3–4 $\mu mol\ O_2\ m^{-2}\ s^{-1}$; Table 1).

Energy budget

Reflectance measurements with a field radiance fibre-optic microprobe revealed that the fraction of the incident light energy absorbed by the mat ecosystem as a whole ranged from 82.5% for the AD mat to 98.3% for the AUS mats respectively (Table 1). The remaining light energy was backscattered and not utilized.

The flux of energy conserved by photosynthesis, J_{PS}, increased linearly with the flux of absorbed light energy under light-limiting conditions and reached saturation at high irradiance, which was similar for all studied mats (1.4–1.8 $J\ m^{-2}\ s^{-1}$; Fig. 3, green symbols in left panels). The inverted exponential model of Webb and colleagues (1974) provided a good fit to the photosynthesis versus absorbed energy data (green curves in Fig. 3, left panels; $R^2 > 0.98$). The initial slope of this fit represented the maximal efficiency with which the absorbed light energy was photochemically conserved in photosynthesis. This maximal efficiency ranged from 4.5% for the AD mat to 16.2% for the AUS mat (Table 1), and was substantially lower than the theoretical maximum of 27.7% as estimated for an ideal photosynthetic system requiring 8 photons to evolve one molecule of O_2 (Al-Najjar *et al.*, 2010).

Excess absorbed light energy was dissipated as heat causing a small temperature increase inside the mat relative to the overlying water (data not shown, but see Al-Najjar *et al.*, 2010). The heat dissipation flux, J_H, increased linearly with the absorbed light energy (Fig. 3, red symbols in left panels). The sum of $J_{PS} + J_H$ was equal (within 2%) to the flux of light energy absorbed by the mat ecosystem (compare red and black lines in left panels in

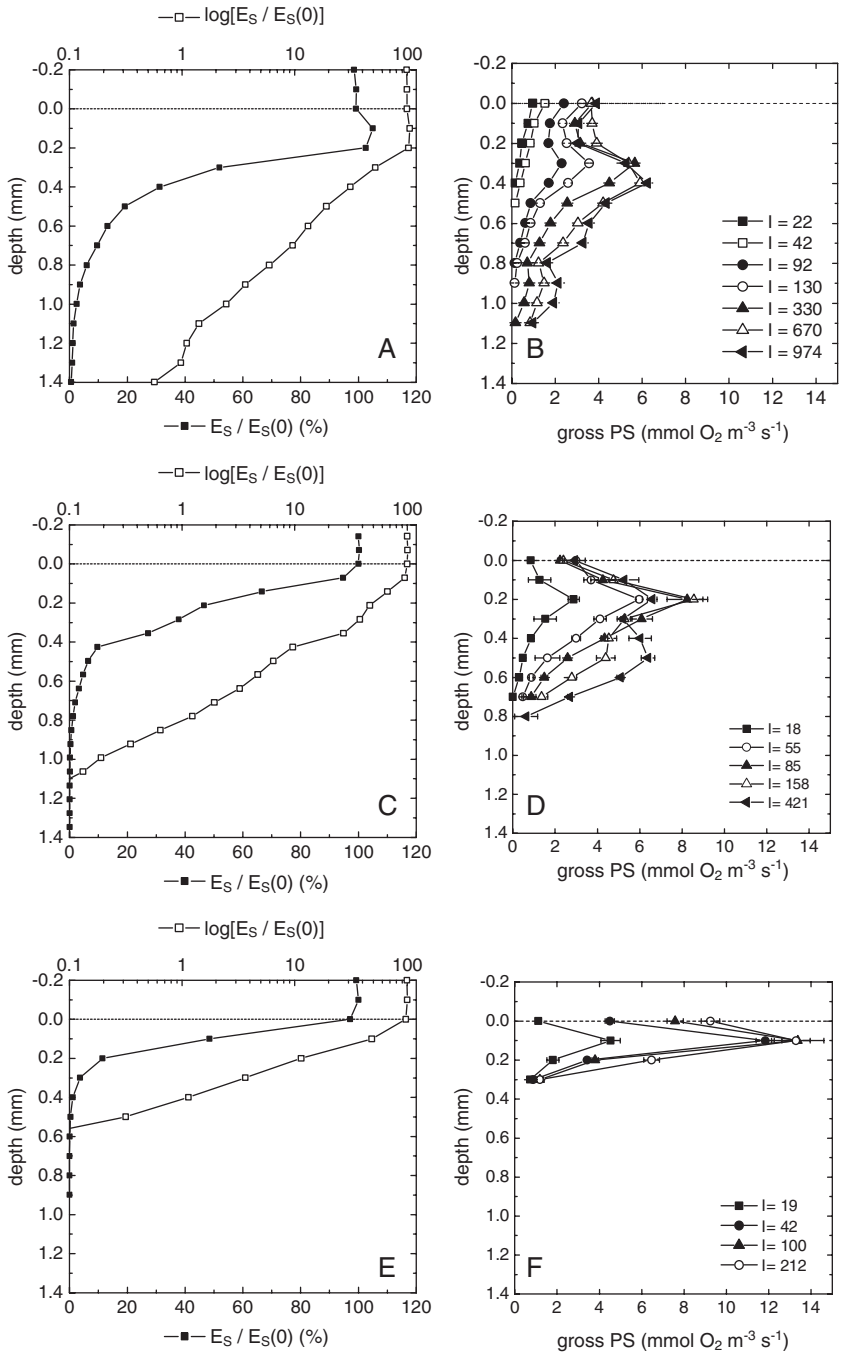

Fig. 2. Vertical profiles of scalar irradiance integrated over PAR (left) and volumetric rates of gross photosynthesis (right) in the AD (A and B), ARC (C and D) and AUS (E and F) mat. Scalar irradiances were normalized to the value measured at the mat surface, and are plotted in linear (filled symbols) and logarithmic (open symbols) scale. Rates of photosynthesis were measured at increasing incident downwelling irradiances shown in legend (in μmol photons m^{-2} s^{-1}). Error bars represent standard errors derived from three measurements at each depth. Dotted horizontal line indicates the mat surface. A and B are reproduced from Al-Najjar and colleagues (2010).

Fig. 3), confirming that the combined measurements of light, O_2 and temperature accounted for all significant fluxes in the light energy budget of the mats.

Overall, heat dissipation dominated the light energy budget in all studied mats. Under light-limiting conditions, where the photosynthetic efficiency was maximal, heat dissipation constituted between 84% (AUS mat) and 96% (AD mat) of the absorbed light energy. At high irradiance, typically experienced by the mats during midday, > 99% of the absorbed light energy was dissipated as heat and thus < 1% was conserved by photosynthesis (Fig. 3, right panels).

Photosynthetic efficiency versus mat characteristics

The maximal photosynthetic efficiency, $\varepsilon_{PS,max}$, determined for each of the studied mats, was most strongly correlated with the light attenuation coefficient ($R^2 = 0.98$; Fig. 4A).

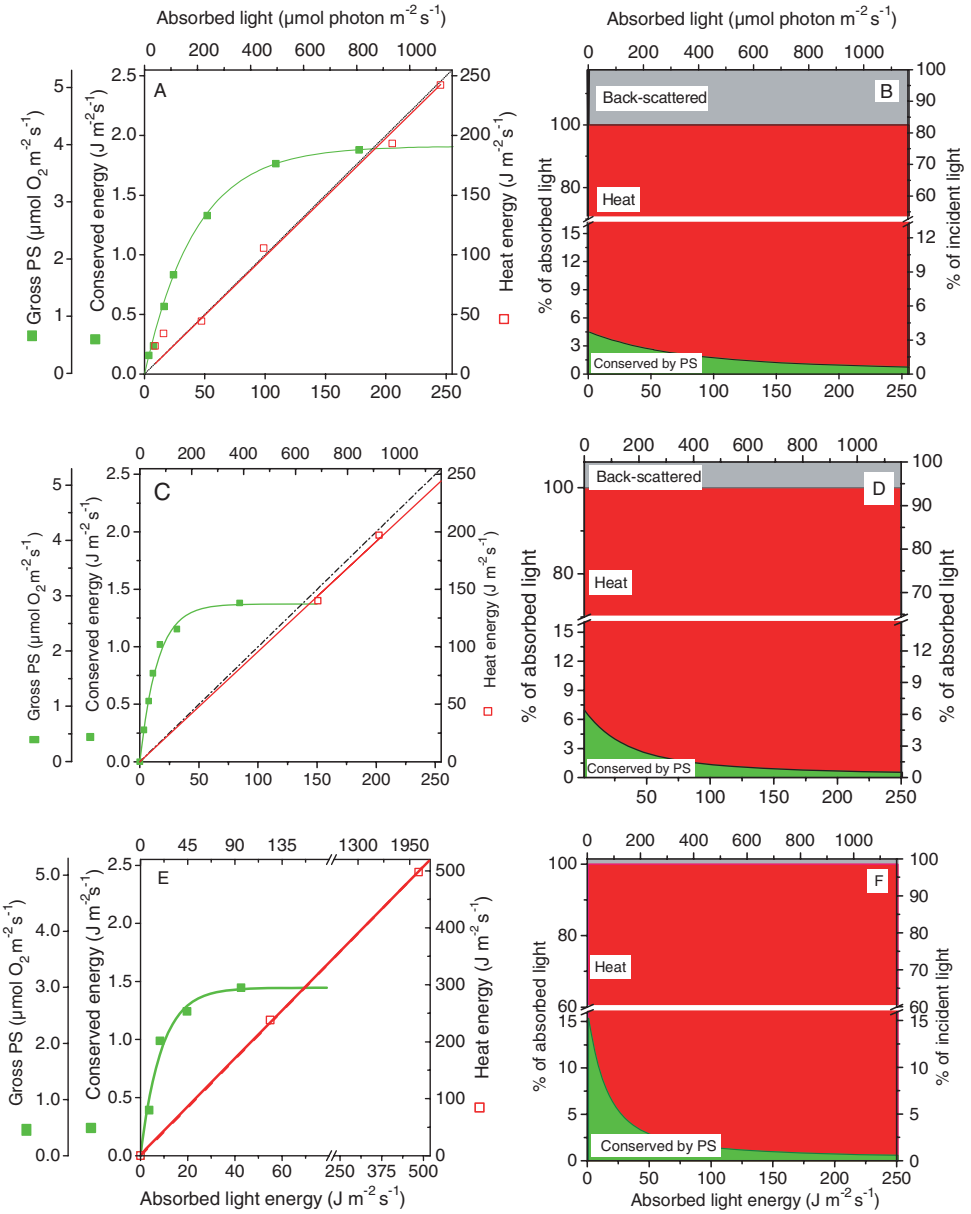

Fig. 3. Left panels: Fluxes of gross photosynthesis, J_{PS}, and heat dissipation, J_H, as a function of the flux of absorbed light energy, J_{abs}. Symbols represent measured values, green curves are fits by the inverted exponential model, red lines are linear fits of the measured $J_{PS} + J_H$ versus J_{abs}, whereas black dotted lines depict the condition of light energy conservation ($J_{PS} + J_H = J_{abs}$). Right panels: energy budgets in the studied microbial mats as a function of absorbed light energy, showing relative contributions of the photosynthetically conserved energy (green), energy dissipated as heat (red) and back-scattered energy (grey). The contributions were normalized to the absorbed (left axis) and incident (right axis) light energy. Top, middle and bottom panels correspond to the AD, ARC and AUS mats respectively. When appropriate, the fluxes are displayed in units of energy (Joule) and quanta (mol). Note the break on the *x*-axis in E and on the *y*-axis in B, D and F.

Significant correlations, although with lower R^2, were also identified between $\varepsilon_{PS,max}$ and the average concentrations of Chl *a* in the euphotic zone ($R^2 = 0.85$; Fig. 4B, filled symbols) and the average concentrations of photopigments (sum of Chl *a* and the accessory pigments PC and FUC) in the euphotic zone ($R^2 = 0.95$; Fig. 4B, open symbols).

Discussion

On a cellular level, the efficiency of light utilization in photosynthetic organisms depends on a variety of factors, including irradiance, temperature, nutrients, salinity, hydration status and pigmentation (Falkowski and Raven, 1997; Flameling and Kromkamp, 1998; Beardall

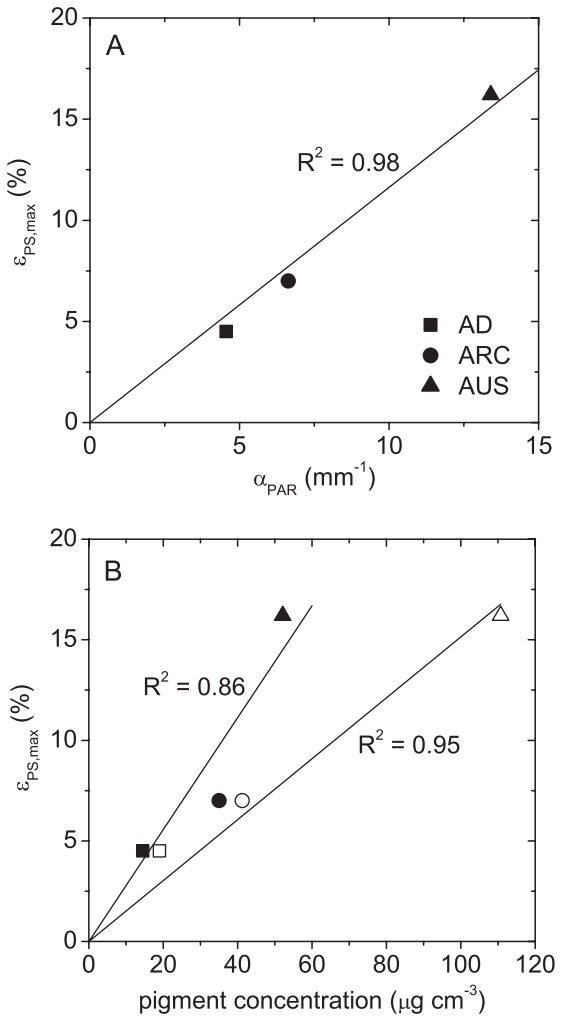

Fig. 4. Maximum photosynthetic efficiency of the studied mats, $\varepsilon_{PS,max}$, as a function of (A) light attenuation coefficient, α_{PAR}, and (B) pigment concentrations in the euphotic zone. Closed and open symbols in panel B correspond to Chl *a* and the sum of Chl *a* and accessory pigments (phycocyanin and fucoxanthin) respectively.

et al., 2001; Abed *et al.*, 2006; Ludwig *et al.*, 2006; Aarti *et al.*, 2007; Chaves *et al.*, 2009). For given environmental conditions, photosynthetic cells employ specific regulatory mechanisms to optimize harvesting and utilization of incident light energy. Considering the large daily fluctuations in light availability, non-photochemical quenching (NPQ) is perhaps the most important short-term regulatory mechanism. Photosynthetic cells use NPQ to protect their photosynthetic apparatus from photo-damage by channelling excess light energy to heat dissipation, resulting in a substantially reduced quantum efficiency and thus saturation of photosynthesis at high irradiance in comparison to light-limiting conditions (Falkowski and Raven, 1997).

Similar to previous studies on photosynthetic microbial mats (e.g. Kühl *et al.*, 1996; Kühl and Fenchel, 2000), our results show that the overall response of a photosynthetic mat ecosystem to increasing irradiance mirrors the response of an individual photosynthetic cell. The photosynthetic efficiency was highest under light-limiting conditions, with a significant part of the absorbed light energy being conserved as chemical energy (4.5–16.2%, depending on the mat). In contrast, at high irradiances typical of midday *in situ* conditions the photosynthetic efficiency decreased below 1% and > 99% of the absorbed light energy was dissipated as heat (Fig. 3, right panels).

In addition to this qualitative similarity, there are also important differences to consider when comparing photosynthetic efficiencies of single cells and mat ecosystems. First, environmental conditions influencing photosynthetic efficiency in mats, most notably light, vary steeply within the euphotic zone. Second, photosynthetic mat ecosystems contain significant amounts of detritus, exopolymers, sand grains and mineral precipitates (Kühl and Fenchel, 2000) that contribute to light absorption but not to photosynthesis. We discuss the consequences of these factors in more details below.

Our results show that photosynthetic efficiency was higher in mats with a shallower and more densely populated euphotic zone (measured as a concentration of photopigments), and that it increased linearly with the attenuation coefficient of PAR in the mat. The latter suggests that the light attenuation coefficient is a good predictor of a microbial mat's efficiency to conserve light energy. The rationale behind this can be understood by considering that in a mixture of photosynthetically active and inactive components, the photosynthetic efficiency and light attenuation are tightly linked through the density and distribution of photopigments that channel light energy into the photosynthetic reaction centres. Higher pigment concentrations, which are indicative of higher photosynthetically active biomass, imply higher volumetric rates of photosynthesis and thus, for a given incident irradiance, higher photosynthetic efficiency. At the same time, when pigment concentrations are higher, light absorption is stronger and occurs within a shallower zone, and the contribution of photopigments to total light absorption in the mat relative to that of photosynthetically inactive components, becomes higher.

Due to strong light attenuation, cells at the top of a mat photosynthesize with lower efficiency than those located only a few tens of micrometers below, because they are partially inhibited by light. On the other hand, although the cells in deeper mat layers photosynthesize with close to maximum efficiency, their growth is likely limited by light. This suggests that, for a given incident irradiance, there is an optimum position or interval of positions below the mat surface, where the available light is not too high to inhibit and not too low to limit photosynthesis. Under these light

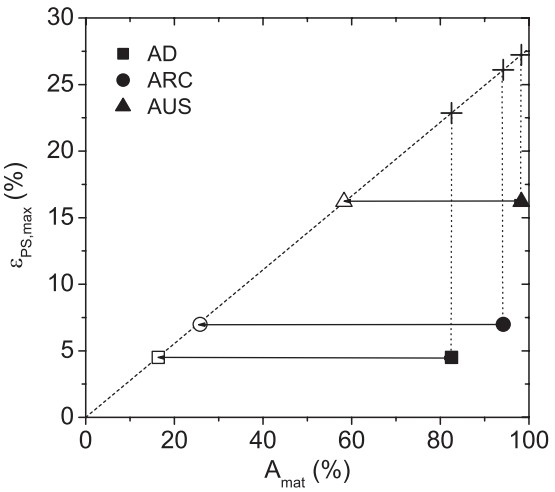

Fig. 5. Maximum photosynthetic efficiency of a mat ecosystem, $\varepsilon_{PS,max}$, as a function of mat absorbance (A_{mat}, calculated as the ratio between the absorbed and incident light energy flux). Filled symbols represent measured data for the three studied mats; crosses represent efficiencies of an ideal photosynthetic ecosystem with the same absorbance as the studied mats. Horizontal arrow between the filled and open symbol represents estimated percentage of incident light energy that is absorbed by photosynthetically inactive components of the respective mat.

conditions, cell growth could be optimal and result in a distinct layer characterized by high density of photosynthetically active cells and thus high volume-specific rates of photosynthesis. Indeed, such a distinct structural and functional layering is typically found in photosynthetic mats (e.g. Fenchel and Kühl, 2000; Jonkers *et al.*, 2003; Al-Najjar *et al.*, 2010; this study).

Generally, the maximal photosynthetic efficiencies in the studied mats were considerably lower than the estimated theoretical maximum of 27.7% (Al-Najjar *et al.*, 2010), indicating that light absorption by photosynthetically inactive components played a significant role in the light energy budget. We estimated the contribution of non-photosynthetic components based on an assumption that the photosynthetically active cells were ideal, i.e., operating with a theoretically maximal quantum efficiency of 1/8 mol O_2 (mol photons)$^{-1}$. The expected efficiency of an ideal photosynthetic ecosystem that absorbs the same fraction of incident light energy as the studied mats (82.5–98.3%; Table 1) is in the range of 23–27% (Fig. 5, crosses), which considerably exceeds the measured mat efficiencies. In contrast, the absorbance of an ideal ecosystem required to obtain the same efficiencies as those measured for the studied mats ranges between 16–58% (Fig. 5, open symbols). By subtracting the measured and required absorbances (horizontal arrows in Fig. 5), we estimated that the contribution of photosynthetically inactive components to total light absorption in the mat ecosystem was up to 73–80% for the AD and ARC mats and about 41% in the AUS mat. These estimates and the measured differences between the studied mats were consistent with the results obtained by combining staining of exopolymeric substances (de Beer *et al.*, 1996) and confocal microscopy, which showed larger amounts of exopolymers relative to photosynthetic cells and a more loosely organized structure in the AD and ARC mats as compared with the AUS mat (Fig. S3).

Our results are consistent with the general patterns and principles of community photosynthesis as discussed by Sand-Jensen and co-workers (Sand-Jensen and Krause-Jensen, 1997; Krause-Jensen and Sand-Jensen, 1998). First, the depth integrated rates of maximal photosynthesis were similar amongst the studied mats (variation of ~18%), although the maximal volumetric rates of photosynthesis averaged over the euphotic zone varied by almost a factor of ~2.5 (Table 1). Similar large variability was observed for chlorophyll concentrations and PAR attenuation. This agrees with the pattern identified for a wide range of aquatic photosynthetic communities, where the increase in volumetric photosynthesis and the decrease in the thickness of the euphotic zone with increasing chlorophyll concentration tend to restrict the variation in depth-integrated photosynthesis by the communities (Krause-Jensen and Sand-Jensen, 1998).

Second, microbial mats are generally less efficient than ecosystems exhibiting a more distinct canopy-like organization of their photosynthetic elements, such as forests, macroalgal stands or corals (Sand-Jensen and Krause-Jensen, 1997; Krause-Jensen and Sand-Jensen, 1998; Gattuso *et al.*, 1999; Hochberg and Atkinson, 2008). Both canopies and mats exhibit strong light attenuation, and individual phototrophic populations will be optimized to the local light regime depending on depth and light exposure. However, light propagation in canopies occurs through a more transparent medium (air or water), and dead biomass does not obstruct light propagation, as most of it falls to the ground or is removed by water flow. Therefore, light is less subject to attenuation by abiotic components in canopies. Conversely, light propagation in microphytobenthic communities is hindered by absorbing and scattering abiotic material and particles. Thus, the effect of photosynthetically inactive absorption of light on overall photosynthetic efficiency in microbial mats is very pronounced.

Comparing the disproportionation of light absorption between photosynthetically active and inactive components, photosynthetic microbial mats are apparently similar to oceanic planktonic systems. This can be inferred by assuming that this disproportionation, when measured at 440 nm (wavelength of maximal absorption of photosynthetic and non-photosynthetic pigments; Bricaud *et al.*, 2010), is representative of the dispropor-

tionation derived for the entire PAR range (this study; Table 1). For example, in the AD mat, the estimated contribution of photosynthetically inactive components to total light absorption in the system (~ 80%) was similar to that found in hyper-oligotrophic waters of the South Pacific Gyre, where the combined contribution of water, non-algal particles (NAP) and coloured dissolved organic material (CDOM) to total absorption is about 75% (Bricaud *et al.*, 2010). On the other side of the extreme, the AUS mat, in which the non-photosynthetic components absorbed about 40% of the light energy, is similar to systems in more eutrophic waters such as the coastal upwelling near Chile, where the combined contribution of water, NAP and CDOM to total absorption is about 50% (Bricaud *et al.*, 2010).

In conclusion, light energy absorbed by photosynthetic mats is primarily channelled to heat dissipation and only a small fraction is conserved as chemical energy via photosynthesis. This fraction depends strongly on the incident irradiance, reaching a maximum at light-limiting conditions and decreasing to < 1% at irradiances typical of mid-day solar exposure. Furthermore, this fraction is significantly decreased due to non-specific light absorption by photosynthetically inactive components of the mat ecosystem such as sediment particles, detritus and exopolymers. Consequently, mats are more efficient when their euphotic zone is thinner, populated with a higher density of photosynthetically active cells and thus characterized by steeper light gradients. In fact, the light attenuation coefficient in the euphotic zone was found to be a very good predictor of the maximum photosynthetic efficiency of a mat ecosystem.

Experimental procedures

Samples

The studied photosynthetic microbial mats originated from Abu Dhabi (AD mat), the Arctic (ARC mat) and Australia (AUS mat). The AD mat was collected from an intertidal flat near Sadeyat Island and incubated in the laboratory at 25°C in 0.2 μm filtered seawater originating from the North Sea (salinity 33). The ARC mat was collected from an intertidal flat in Ymerbukta, Svalbard, and incubated at 4°C in water from the collection site (salinity 34; see Gihring *et al.*, 2010). The AUS mat was collected from the low intertidal zone of the Exmouth Gulf (see Lovelock *et al.*, 2010). It was incubated in seawater North Sea (salinity 33) at 28°C, which circulated over the mat for 5 hours per day to mimic the site-specific environmental conditions. All mats were kept under a 10 h/14 h light/dark illumination regime at incident irradiances of 480 (AD mat), 15 (ARC mat) and 120 μmol photons m^{-2} s^{-1} (AUS mat). Measurements were conducted between 3 weeks and 2 months after sample collection. Phototrophic communities in the mats were dominated by cyanobacteria in the AD and AUS mats and cyanobacteria together with diatoms in the ARC mat (see Fig. S3).

Pigment analysis

Pigments in the mat samples were measured semi-quantitatively using hyperspectral reflectance imaging and quantitatively using spectrophotometry and liquid chromatography on pigment extracts. In hyperspectral imaging, pigments were identified based on their *in vivo* absorption maxima and localized by calculating in every pixel of the image the second derivative of the spectral reflectance at the corresponding wavelength of maximal absorption, i.e. minimal reflectance (Polerecky *et al.*, 2009).

The spectrophotometric quantification of PC followed the procedure described by Sode and colleagues (1991). The uppermost 2 mm of the mats were freeze-dried sample suspended in 1 ml of 65 mM phosphate buffer (pH 8.2) with added lysozyme (62970, Fluka, Switzerland; concentration of 15 mg ml^{-1}) and incubated for 2 h at 37°C. Afterwards, the lysate was centrifuged at 3000 *g* for 20 min at 4°C, followed by the measurement of supernatant absorbance in a spectrophotometer (Lambda 20, Perkin Elmer, USA).

Chlorophyll *a* and FUC concentrations were quantified with high-performance liquid chromatography (HPLC). Mat samples were freeze-dried, horizontally sliced in 200 μm thick sections and dark incubated for 24 h at –20°C in 100% acetone. Subsequently, the supernatant was filtrated through a 0.45 μm Acrodiscs CR 4-mm syringe filter (Pall Gelman Laboratory, USA) and the filtrates were injected into a reverse-phase HPLC consisting of a Waters 996 photo diode array detector (PDA) and a Waters 2695 separation module (Waters, MA). Pigments were separated according to the method described by Wright and colleagues (1991). Identification and quantification were done by comparing the retention time and absorption spectrum of the eluents with those of pigment standards (DHI Water and Environment, Denmark).

Energy fluxes and efficiencies

Measurements and calculations followed the protocols developed by Al-Najjar and colleagues (2010). Briefly, a mat sample was placed in a flow-chamber and vertically illuminated with a collimated light beam of photosynthetically active radiation (PAR, 400–700 nm). A steady laminar flow of seawater (salinity 33) above the mat surface was maintained using a submersed water pump connecting the flow chamber to an aerated water reservoir. Temperature was controlled by recirculating the pumped seawater through a container placed in a thermostat, and was adjusted with an accuracy of 0.05°C to 23°C for the AD and AUS mats and 4°C for the ARC mat.

Volume-specific rates of gross photosynthesis in the mats were measured by the microsensor-based light-dark shift method (Revsbech and Jørgensen, 1983) using a fast-responding O_2 microelectrode (tip diameter 20 μm; Revsbech, 1989). The rates were depth integrated to calculate the areal rate of photosynthesis, P_a, from which the flux of energy conserved by photosynthesis was calculated as

$$J_{PS} = P_a E_G. \quad (1)$$

Here $E_G = 482.9$ kJ $(\text{mol } O_2)^{-1}$ is the energy gained and stored in the light-dependent reactions of photosynthesis, where O_2 is formed by splitting of water, reducing equivalents

are used to form NADPH, and ATP is formed by the proton-motive force (Al-Najjar *et al*., 2010).

Steady-state temperature microprofiles were measured using a thermocouple microsensor (tip diameter ~ 50 μm; T50, Unisense A/S, Denmark) connected to an electric thermometer. From these measurements the flux of heat dissipation was calculated as

$$J_H = \kappa(\partial T/\partial z), \quad (2)$$

where $(\partial T/\partial z)$ is the temperature gradient in the thermal boundary layer and $\kappa = 0.6$ J m^{-1} s^{-1} K^{-1} is thermal conductivity of water (Young *et al*., 1996).

Light penetration in the mats was measured with a scalar irradiance microprobe (integrating sphere diameter 100 μm; Lassen *et al*. 1992). The exponentially decreasing part of the measured profile was used to calculate the attenuation coefficient of scalar irradiance. Spectrally resolved downwelling irradiance, I_λ, was measured with a cosine collector connected to a spectrometer (USB2000, Ocean Optics), which was intercalibrated against a PAR quantum irradiance sensor (LI-250, LI-COR Biosciences). Spectral reflectance of the mats, R_λ, was estimated as $R_\lambda = I_{\lambda,mat}/I_{\lambda,ref}$, where $I_{\lambda,mat}$ and $I_{\lambda,ref}$ are back-scattered spectral radiances measured with an fibre-optic field radiance microprobe (fibre tip diameter 50 μm; Jørgensen and des Marais 1988; Kühl, 2005) above the mat surface and above a white reflectance standard respectively. Subsequently, the flux of absorbed light energy in the PAR region was calculated as

$$J_{abs} = \int I_\lambda E_\lambda (1 - R_\lambda)\, d\lambda, \quad (3)$$

where E_λ is the molar energy content of light with wavelength λ (see more details in Al-Najjar *et al*., 2010). Light, O_2 and temperature measurements were done in the same spot in the mat, the latter two conducted sequentially after a steady-state at a given incident irradiance was reached.

The fluxes of photosynthetically conserved energy, J_{PS}, were plotted against the fluxes of light energy absorbed by the mat, J_{abs}, and fitted with an inverted exponential model (Webb *et al*., 1974). This fit was subsequently used to calculate the efficiency of photosynthetic energy conservation for a continuous range of J_{abs} values as $\varepsilon_{PS} = J_{PS}/J_{abs}$. Of specific interest was the maximum photosynthetic efficiency, $\varepsilon_{PS,max}$, which was derived from the fitted value of ε_{PS} at light-limiting conditions ($J_{abs} \rightarrow 0$; see Al-Najjar *et al*., 2010). After experimentally validating that $J_{abs} = J_{PS} + J_H$, the efficiency of heat dissipation was calculated from the photosynthetic efficiency as $\varepsilon_H = 1 - \varepsilon_{PS}$.

Acknowledgements

We thank Dr Alistair Grinham and Dr Cathrine Lovelock for providing mat samples from Exmouth Gulf, Australia, Joana Sawicka for collecting the Arctic mat samples, Dr Martin Beutler for his assistance with confocal laser microscopy, Dr Katharina Kohls, Judith Klatt and Olivera Svitlica for laboratory assistance, and the technical assistants of the microsensor group for the preparation of microsensors. We are grateful for financial support by the Max-Planck Society and Yusef Jameel Scholarship.

References

Aarti, D., Tanaka, R., Ito, H., and Tanaka, A. (2007) High light inhibits chlorophyll biosynthesis at the level of 5-aminolevulinate synthesis during de-etiolation in cucumber (*Cucumis sativus*) cotyledons. *Photochem Photobiol* **83:** 171–176.

Abed, R.M.M., Polerecky, L., Al Najjar, M., and de Beer, D. (2006) Effect of temperature on photosynthesis, oxygen consumption and sulfide production in an extremely hypersaline cyanobacterial mat. *Aquat Microb Ecol* **44:** 21–30.

Al-Najjar, M.A.A., de Beer, D., Jørgensen, B.B., Kühl, M., and Polerecky, L. (2010) Conversion and conservation of light energy in a photosynthetic microbial mat ecosystem. *ISME J***4:** 440–449.

Beardall, J., Young, E., and Roberts, S. (2001) Approaches for determining phytoplankton nutrient limitation. *Aquat Sci* **63:** 44–69.

de Beer, D., Oflaharty, V., Thaveesri, J., Lens, P., and Verstraete, W. (1996) Distribution of extracellular polysaccharides and flotation of anaerobic sludge. *Appl Microbiol Biotechnol* **46:** 197–201.

Bricaud, A., Babin, M., Claustre, H., Ras, J., and Tieche, F. (2010) Light absorption properties and absorption budget of Southeast Pacific waters. *J Geophys Res* **115:** 1–19.

Chaves, M.M., Flexas, J., and Pinheiro, C. (2009) Photosynthesis under drought and salt stress: regulation mechanisms from whole plant to cell. *Ann Bot* **103:** 551–560.

Des Marais, D.J. (2003) Biogeochemistry of hypersaline microbial mats illustrates the dynamics of modern microbial ecosystems and the early evolution of the biosphere. *Biol Bull* **204:** 160–167.

Dillon, J.G., Miller, S., Bebout, B., Hullar, M., Pinel, N., and Stahl, D.A. (2009) Spatial and temporal variability in a stratified hypersaline microbial mat community. *FEMS Microbiol Ecol* **68:** 46–58.

Epping, E., and Kühl, M. (2000) The responses of photosynthesis and oxygen consumption to short-term changes in temperature and irradiance in a cyanobacterial mat (Ebro Delta, Spain). *Environ Microbiol* **2:** 465–474.

Falkowski, P.G., and Raven, J.A. (1997) *Aquatic Photosynthesis: Blackwell Science*. Washington, DC, USA: Capital City Press.

Fenchel, T., and Kühl, M. (2000) Artificial cyanobacterial mats: growth, structure, and vertical zonation patterns. *Microb Ecol* **40:** 85–93.

Ferris, M.J., Nold, S.C., Revsbech, N.P., and Ward, D.M. (1997) Population structure and physiological changes within a hot spring microbial mat community following disturbance. *Appl Environ Microbiol* **63:** 1367–1374.

Flameling, I.A., and Kromkamp, J. (1998) Light dependence of quantum yields for PSII charge separation and oxygen evolution in eucaryotic algae. *Limnol Oceanogr* **43:** 284–297.

Foster, J.S., Green, S.J., Ahrendt, S.R., Golubic, S., Reid, R.P., Hetherington, K.L., and Bebout, L. (2009) Molecular and morphological characterization of cyanobacterial diversity in the stromatolites of Highborne Cay, Bahamas. *ISME J* **3:** 573–587.

Gattuso, J.P., Allemand, D., and Frankignoulle, M. (1999) Photosynthesis and calcification at cellular, organismal and

community levels in coral reefs: a review on interactions and control by carbonate chemistry. *Am Zool* **39:** 160–183.
van Gemerden, H. (1993) Microbial mats: a joint venture. *Mar Geol* **113:** 3–25.
Gihring, T.M., Lavik, G., Kuypers, M.M.M., and Kostka, J.E. (2010) Direct determination of nitrogen cycling rates and pathways in Arctic fjord sediments (Svalbard, Norway). *Limnol Oceanogr* **55:** 740–752.
Hochberg, E.J., and Atkinson, M.J. (2008) Coral reef benthic productivity based on optical absorptance and light-use efficiency. *Coral Reefs* **27:** 49–59.
Jensen, S.I., Stenou, A.-S., Bhaya, D., Kühl, M., and Grossman, A.R. (2011) *In situ* dynamics of O_2, pH and cyanobacterial transcripts associated with CCM, photosynthesis and detoxification of ROS. *ISME J* **5:** 317–328.
Jonkers, H.M., Ludwig, R., De Wit, R., Pringault, O., Muyzer, G., Niemann, H., *et al*. (2003) Structural and functional analysis of a microbial mat ecosystem from a unique permanent hypersaline inland lake: 'La Salada de Chiprana' (NE Spain). *FEMS Microbiol Ecol* **44:** 175–189.
Jonkers, H.M., Koh, I.O., Behrend, P., Muyzer, G., and de Beer, D. (2005) Aerobic organic carbon mineralization by sulfate-reducing bacteria in the oxygen-saturated photic zone of a hypersaline microbial mat. *Microb Ecol* **49:** 291–300.
Jørgensen, B.B., and des Marais, D.J. (1988) Optical-properties of benthic photosynthetic communities—fiber-optic studies of cyanobacterial mats. *Limnol Oceanogr* **33:** 99–113.
Jørgensen, B.B., Cohen, Y., and Des Marais, D.J. (1987) Photosynthetic action spectra and adaptation to spectral light-distribution in a benthic cyanobacterial mat. *Appl Environ Microbiol* **53:** 879–886.
Krause-Jensen, D., and Sand-Jensen, K. (1998) Light attenuation and photosynthesis of aquatic plant communities. *Limnol Oceanogr* **43:** 396–407.
Kühl, M. (2005) Optical microsensors for analysis of microbial communities. *Methods Enzymol* **397:** 166–199.
Kühl, M., and Fenchel, T. (2000) Bio-optical characteristics and the vertical distribution of photosynthetic pigments and photosynthesis in an artificial cyanobacterial mat. *Microb Ecol* **40:** 94–103.
Kühl, M., Glud, R.N., Ploug, H., and Ramsing, N.B. (1996) Microenvironmental control of photosynthesis and photosynthesis-coupled respiration in an epilithic cyanobacterial biofilm. *J Phycol* **32:** 799–812.
Lassen, C., Ploug, H., and Jørgensen, B.B. (1992) A fiberoptic scalar irradiance microsensor—application for spectral light measurements in sediments. *FEMS Microbiol Ecol* **86:** 247–254.
Lovelock, C., Grinham, A., Adame, M.F., and Penrose, H. (2010) Elemental composition and productivity of cyanobacterial mats in an arid zone estuary in north Western Australia. *Wetlands Ecol Manage* **18:** 37–47.
Ludwig, R., Pringault, O., de Wit, R., de Beer, D., and Jonkers, H.M. (2006) Limitation of oxygenic photosynthesis and oxygen consumption by phosphate and organic nitrogen in a hypersaline microbial mat: a microsensor study. *FEMS Microbiol Ecol* **57:** 9–17.
Polerecky, L., Bissett, A., Al-Najjar, M., Faerber, P., Osmers, H., Suci, P.A., *et al*. (2009) Modular spectral imaging system for discrimination of pigments in cells and microbial communities. *Appl Environ Microbiol* **75:** 758–771.
Revsbech, N.P. (1989) An oxygen microsensor with a guard cathode. *Limnol Oceanogr* **34:** 474–478.
Revsbech, N.P., and Jørgensen, B.B. (1983) Photosynthesis of benthic microflora measured with high spatial-resolution by the oxygen microprofile method - capabilities and limitations of the method. *Limnol Oceanogr* **28:** 749–756.
Sand-Jensen, K., and Krause-Jensen, D. (1997) Broad-scale comparison of photosynthesis in terrestrial and aquatic plant communities. *Oikos* **80:** 203–208.
Sode, K., Horikoshi, K., Takeyama, H., Nakamura, N., and Matsunaga, T. (1991) Online monitoring of marine cyanobacterial cultivation based on phycocyanin fluorescence. *J Biotechnol* **21:** 209–217.
Steunou, A.-S., Jensen, S.I., Brecht, E., Becraft, E.D., Bateson, M.M., Kilian, O., *et al*. (2008) Regulation of nif gene expression and the energetics of N2 fixation over the diel cycle in a hot spring microbial mat. *ISME J* **2:** 364–378.
Teske, A., and Stahl, D.A. (2001) Microbial mats and biofilms: evolution, structure and function of fixed microbial communities. In *Biodiversity of Microbial Life: Foundation of Earth's Biosphere*. Staley, J.T., and Reysenbach, A.-L. (eds). New York, USA: John Wiley and Sons, pp. 49–100.
Visscher, P.T., and Stolz, J.F. (2005) Microbial mats as bioreactors: populations, processes, and products. *Palaeogeogr Palaeoclimatol Palaeoecol* **219:** 87–100.
Ward, D.M., Bateson, M.M., Ferris, M.J., Kühl, M., Wieland, A., Koeppel, A., and Cohan, F.M. (2006) Cyanobacterial ecotypes in the microbial mat community of Mushroom Spring (Yellowstone National Park, Wyoming) as species-like units linking microbial community composition, structure and function. *Philos Trans R Soc Lond B Biol Sci* **361:** 1997–2008.
Webb, W.L., Newton, M., and Starr, D. (1974) Carbon-dioxide exchange of *Alnus-Rubra* – mathematical-model. *Oecologia* **17:** 281–291.
Wright, S.W., Jeffrey, S.W., Mantoura, R.F.C., Llewellyn, C.A., Bjornland, T., Repeta, D., and Welschmeyer, N. (1991) Improved HPLC method for the analysis of chlorophylls and carotenoids from marine-phytoplankton. *Mar Ecol Prog Ser* **77:** 183–196.
Young, H.D., Freedman, R.A., and Ford, L. (1996) *University Physics, with Modern Physics*. Boston, MA, USA: Addison Wesley.

Supporting information

Additional Supporting Information may be found in the online version of this article.

Fig. S1. Hyperspectral imaging of vertical sections of the (A) AD, (B) ARC and (C) AUS mats. Left panels: true-colour images. The scale bar is 1 mm. Right panels: reflectance spectra from selected points in the images calculated from the second derivative of the measured reflectance spectra at the wavelengths of maximal absorption. Note the significant amounts of bacteriochlorophyll *a* in deeper part of AD mat (region number 2). In addition to Chl *a* and PC, significant amounts of bacteriochlorophyll *a*, which is a characteristic pigment of anoxygenic phototrophs, were detected at depths

> 1.5 mm in the AD mat based on the characteristic absorption maxima at 802 and 870 nm.

Fig. S2. False-colour images of photosynthetic cells and exopolymers inside the (A) Abu-Dhabi, (B) Arctic and (C) Australian mats obtained by confocal laser microscopy. Z-stack extending over the top 300 μm were acquired in 10 μm steps and analysed with the ImageJ software (Abramoff *et al.*, 2004). Blue, red and green colour corresponds to Chl *a*, PC and the EPS-bound dye fluorescent brightener 28 respectively. The scale bar is 200 μm.

Fig. S3. Microscopic images of the cyanobacteria and diatoms found in the studied mats. A–G: AD mat, H–L: ARC mat, M–T: AUS mat. The probable taxons are: A: *Aphanothece* sp.1; B: *Chroococcidiopsis* sp.; C: *Leptolyngbya* sp.1; D: *Microcoleus* sp.1; E: *Euhalothece* sp.; F: *Aphanothece* sp.2; G: *Aphanocapsa* sp.; H: *Oscillatoria* sp.2; I: *Phormidium* sp.; J: *Nitzschia* sp.; K: (not identified); L: *Calothrix* sp.; M: *Phoramidium* sp.; N: *Leptolyngbya* sp.2; O: *Microcoleus chthonoplastes*; P: *Microcoleus* sp.2; Q: *Oscillatoria* sp.1; R: *Anabaena* sp.; S: *Symploca muscorum*; T: *Leptolyngbya* sp.3. The scale bar in all the images is 5 μm.